Quantifying submerged fluvial topography using hyperspatial resolution UAS imagery and structure from motion photogrammetry

Journal:	*Earth Surface Processes and Landforms*
Manuscript ID:	ESP-13-0368.R3
Wiley - Manuscript type:	Paper
Date Submitted by the Author:	n/a
Complete List of Authors:	Woodget, Amy; University of Worcester, Institute of Science and Environment Carbonneau, Patrice; Durham University, Department of Geography Visser, Fleur; University of Worcester, Institute of Science and Environment Maddock, Ian; University of Worcester, Institute of Science and Environment
Keywords:	unmanned aerial system, structure-from-motion photogrammetry, fluvial, submerged topography, bathymetry

Quantifying submerged fluvial topography using hyperspatial resolution UAS imagery and structure from motion photogrammetry

A.S. Woodget[1], P.E. Carbonneau[2], F. Visser[1] and I. Maddock[1]

[1] Institute of Science and Environment, University of Worcester, Henwick Grove, Worcester, WR2 6AJ, UK, [2] Department of Geography, University of Durham, South Road, Durham, DH1 3LE, UK,

Keywords: unmanned aerial system, structure from motion, photogrammetry, fluvial, submerged topography, bathymetry

Abstract

Quantifying the topography of rivers and their associated bedforms has been a fundamental concern of fluvial geomorphology for decades. Such data, acquired at high temporal and spatial resolutions, are increasingly in demand for process-oriented investigations of flow hydraulics, sediment dynamics and in-stream habitat. In these riverine environments, the most challenging region for topographic measurement is the wetted, submerged channel. Generally, dry bed topography and submerged bathymetry are measured using different methods and technology. This adds to the costs, logistical challenges and data processing requirements of comprehensive river surveys. However, some technologies are capable of measuring the submerged topography. Through-water photogrammetry and bathymetric LiDAR are capable of reasonably accurate measurements of channel beds in clear water. Whilst the cost of bathymetric LiDAR remains high and its resolution relatively coarse, the recent developments in photogrammetry using Structure from Motion (SfM) algorithms promise a fundamental shift in the

accessibility of topographic data for a wide range of settings. Here we present results demonstrating the potential of so called SfM-photogrammetry for quantifying both exposed and submerged fluvial topography at the mesohabitat scale. We show that imagery acquired from a rotary-winged Unmanned Aerial System (UAS) can be processed in order to produce digital elevation models (DEMs) with hyperspatial resolutions (c. 0.02m) for two different river systems over channel lengths of 50-100m. Errors in submerged areas range from 0.016m to 0.089m, which can be reduced to between 0.008m and 0.053m with the application of a simple refraction correction. This work therefore demonstrates the potential of UAS platforms and SfM-photogrammetry as a single technique for surveying fluvial topography at the mesoscale (defined as lengths of channel from c.10m to a few hundred metres).

1. Introduction

1.1 Importance of quantifying fluvial topography

Topography is the most basic descriptor of geomorphology and one of the most often used predictors of geomorphic process. The quantification of exposed and submerged fluvial topography at high spatial and temporal resolutions is increasingly in demand for a wide range of science and management applications, including geomorphic change detection (Wheaton et al., 2010; Bangen et al., 2013; Legleiter, 2014a; Legleiter 2014b), hydraulic modelling, physical habitat assessment (Maddock, 1999), river restorations and sediment budgeting (Hicks, 2012; Marcus et al., 2012).

These applications require a technique for quantifying fluvial topography which is objective, repeatable and spatially explicit. The data should be high resolution and spatially continuous in three dimensions, rather than simple point or line sampling

(Fausch et al., 2002; Mertes, 2002; Wiens, 2002; Orr et al., 2008; Fernandez et al., 2011; Carbonneau et al., 2012; Nestler et al., 2013). The practicality of data collection and cost are also important. An approach which meets these needs has potential for characterising fluvial topography and therefore also physical habitat in accordance with the 'riverscape' concept (see Fausch et al., 2002; Ward et al., 2002; Wiens, 2002; Carbonneau et al., 2012). This paradigm advocates a shift from understanding rivers as gradually changing longitudinal elements of a wider terrestrial landscape (as per Vannote et al., 1980's River Continuum Concept) to those characterised by high spatial and temporal heterogeneity (Ward, 1998; Lapointe, 2012), and makes this heterogeneity the focus of assessment (Ward, 1998; Fausch et al., 2002; Legleiter et al., 2014b).

Within this paper, we briefly review existing approaches for quantifying the spatial heterogeneity of fluvial topography. We then introduce and quantitatively assess an alternative approach, using high resolution unmanned aerial system (UAS) imagery and Structure-from-Motion (SfM) photogrammetry. Our approach considers both exposed and submerged parts of the channel and is focussed on obtaining data at the mesoscale. We define the mesoscale as covering lengths of channel from c.10m to a few hundred metres. This is generally acknowledged as an ecologically meaningful scale for physical habitat assessments (Frissell et al., 1986, Newson and Newson 2000, Fausch et al., 2002, Frothingham et al., 2002, Nestler et al., 2013).

1.2 Existing approaches

Traditional approaches to quantifying fluvial topography typically use tape measures, depth poles, levelling equipment, total stations or GNSS (Global Navigation Satellite Systems). Such surveys offer a single technique for quantifying both exposed and

(shallow) submerged topography. However, these methods are time consuming, labour intensive, provide limited spatial extent (Winterbottom and Gilvear 1997; Feurer et al., 2008, Bangen et al., 2013) and do not provide the continuous spatial coverage needed to characterise the spatial heterogeneity of the 'riverscape' (Westaway et al., 2001; Marcus, 2012). This 'riverscape' perspective is gaining increasing support within river science and management (Fernandez et al., 2011; Bergeron and Carbonneau 2012; Carbonneau et al., 2012) and precipitates a need for different ways of quantifying fluvial topography.

In recent years, remote sensing approaches have emerged as alternatives to traditional methods of quantifying fluvial topography. Remote sensing offers an efficient approach to cover large areas with continuous data coverage, which cannot be achieved by point or line sampling. Here we briefly review well established passive techniques including (1) the spectral-depth relationship approach and (2) digital photogrammetry, and the more recent, active remote sensing methods of (3) airborne, bathymetric and terrestrial laser scanning.

Spectral-Depth Approach

The spectral-depth approach is perhaps the most widely used method for quantifying flow depth within submerged areas. An empirical correlation is established between flow depth data acquired in the field and corresponding image spectral properties. The correlation is applied to the remainder of the image to provide spatially continuous water depth datasets without great expense (which can then be converted to topographic data). This approach is capable of producing topographic outputs at spatial resolutions of c. 0.05m and mean errors of c. 0.10m for mean water depths of less than 1m (Lejot et al., 2007) (Table 1), and thus is well suited to

studies at the mesoscale. However, significant field efforts are still required for the collection of empirical depth data, which must represent the range of depths present within the area of interest. As a consequence, data collection is time-consuming and labour intensive and results are site and image specific. Results are also known to be adversely affected by variations in scene illumination, substrate, turbidity and water surface roughness (Winterbottom and Gilvear 1997; Westaway et al., 2003; Legleiter et al., 2004; Carbonneau et al., 2006; Lejot et al., 2007; Legleiter et al., 2009; Bergeron and Carbonneau 2012; Legleiter, 2012). The maximum water depth limit achieved using spectral-depth approaches is reported to be up to 1m (Carbonneau et al., 2006; Legleiter et al., 2004; Legleiter et al., 2009, Legleiter, 2012).

Digital Photogrammetry

Lane (2000) reviews the progress made in the use of photogrammetry for river channel research prior to the year 2000. Today, the use of digital photogrammetry is well-established for the rapid generation of topographic datasets within fluvial settings (Lane, 2000; Westaway et al., 2001; Carbonneau et al., 2003; Lane et al., 2010). Collinearity equations, which relate the 2D co-ordinates within a camera to the 3D co-ordinates of the scene, are solved to produce continuous topographic datasets. Resulting DEM spatial resolutions are reported to be c. 0.05m with mean errors of c. 0.10m from aerial platforms (Lejot et al., 2007; Lane et al., 2010) (Table 1), and close-range photogrammetry readily reaching sub-cm spatial resolutions (e.g. Butler et al., 2001). Digital photogrammetry is thus suitable for studies addressing the mesoscale and has seen widespread application to exposed terrain. However, there has been limited application of digital photogrammetry in submerged parts of the fluvial environment, perhaps due to the adverse effects of turbidity and

water surface roughness, and issues relating to maximum light penetration depth. These effects have been found to reduce the accuracy of the results in submerged areas or preclude the approach entirely (Westaway et al., 2001; Feurer et al., 2008; Marcus, 2012).

The complicating effects of light refraction at the air-water interface also require consideration in through-water photogrammetry. The geometry of this refraction is described by Snell's Law (Equation 1) and shown in Figure 1;

$$\frac{\sin r}{\sin i} = \frac{h}{h_A} = n$$

Equation (1)

Where *r* is the angle of the refracted light ray below the water surface, *i* is the angle of the incident light ray above the water surface, *h* is the true water depth, h_A is the apparent water depth and *n* is the refractive index of water. For clear water, this refractive index has a value of 1.34, which varies by less than 1% for a range of temperature and salinity conditions (Jerlov, 1976; Westaway et al., 2001; Butler et al., 2002). Without the application of a correction procedure, this two-media refraction problem results in the overestimation of true bed elevation (i.e. an underestimation of water depth), as shown in Figure 1 (Fryer, 1983; Fryer and Kneist 1985; Butler et al., 2002; Westaway et al., 2001). However, with the knowledge of apparent water depth (h_A) and the refractive index of water (*n*), the true depth (*h*) can be estimated using a simple refraction correction, as shown in Equation 2;

$$h = n \times h_A$$

Equation (2)

This simple correction procedure has been used to adjust digital photogrammetric outputs for submerged parts of the fluvial environment, as shown by Westaway et al., (2000, 2001). Results of these studies showed an improvement in mean error following refraction correction, and for depths less than 0.4m mean error became comparable with that of exposed terrain. However, larger errors were observed at depths beyond 0.4m which scaled with depth (Westaway et al., 2000). A more complex correction procedure, where the camera position and water surface elevation were also considered, did not significantly improve the results and yet increased computation times. It was noted that clear and relatively shallow waters produced the most accurate results (Westaway et al., 2000; Westaway et al., 2001; Feurer et al., 2008). Refraction correction approaches have subsequently been applied elsewhere (e.g. Lane et al., 2010), further highlighting the potential of the procedure for quantifying submerged fluvial topography.

Laser Scanning

The use of laser scanning systems for topographic surveying has seen rapid growth since the early 2000s. Accurate elevation data can be acquired for exposed terrain. However, the use of near-infrared light, which is strongly absorbed in water, usually makes quantification of submerged topography impossible (Lane and Carbonneau 2007; Legleiter, 2012). Recently, the emergence of airborne blue-green or bathymetric laser scanners has provided a potential solution (e.g. Kinzel et al., 2007; McKean et al., 2009; Bailly et al., 2010). Blue-green scanning approaches are less affected by turbidity and water surface roughness than passive remote sensing techniques (Marcus, 2012), and are capable of surveying much greater water depths (Bailly et al., 2010; Kinzel et al., 2013). At present however, the application of airborne bathymetric laser scanning to the mesoscale study of fluvial environments is

severely limited by high cost, restricted sensor availability, coarse spatial resolution and a lack of reliability in shallower waters (McKean et al., 2009; Bailly et al., 2012; Hicks, 2012; Legleiter, 2012; Marcus, 2012; Kinzel et al., 2013).

Terrestrial laser scanners (TLS) provide another method for fluvial topographic surveying, known for providing much higher spatial resolutions (c. 0.01m) with low mean errors (0.004m-0.030m) in exposed areas (Heritage and Hetherington 2007; Bangen et al., 2013) (Table 1). As such, they are better suited to mesoscale assessments of topography. However, data collection is time consuming and labour intensive, spatial coverage is limited by scanner range and the scanners themselves remain costly to acquire (Bangen et al., 2013).

Recent publications have provided some initial testing of green wavelength (λ =532nm) TLS for surveying submerged areas (Smith et al., 2012; Smith and Vericat 2013). The strongly oblique TLS scan angles mean that refraction effects are significant. The recent work of Smith and Vericat (2013) has provided one of the first field tests of this approach, representing an important advance in the applied use of TLS in submerged areas. TLS potentially provides a single technique capable of surveying both exposed and shallow submerged areas. However, further testing in different settings is needed. TLS is not yet capable of providing centimetre resolution topographic data over mesoscale lengths of channel, at least not without significant and time consuming field efforts.

Combined Approaches

Some studies have tried to overcome the limitations of using a single approach by combining different techniques to quantify the topography of both exposed and submerged terrain (e.g. Westaway et al., 2003; Lane et al., 2010; Legleiter, 2012;

Williams et al., 2013; Javernick et al., 2014). However, this adds to the costs, logistical challenges and data processing requirements. To our knowledge, the work of Westaway et al., (2001) using digital photogrammetry, and Smith and Vericat (2013) using TLS are the only studies which have used a single technique over mesoscale lengths of channel. Yet neither of these approaches has been shown to provide hyperspatial resolution topographic data (<0.1m) over these mesoscale extents.

1.3 Emergence of UAS and SfM-photogrammetry

Very recently, the emergence of small unmanned aerial systems (UAS) and parallel developments in software capable of processing their imagery has further contributed to the field of topographic remote sensing. Small UAS include a range of platforms (typically less than 7kg in weight) including fixed- and rotary-winged aircraft, kites and balloons. Initial studies have been carried out for a range of topographic applications, including archaeology (e.g. Eisenbeiss et al., 2005), glacial, paraglacial and aeolian landforms (e.g. Smith et al., 2009; Hugenholtz et al., 2013), landslides (e.g. Niethammer et al., 2012) and within fluvial environments (e.g. Lejot et al., 2007; Hervouet et al., 2011; Fonstad et al., 2013). These studies have suggested that data acquisition with a UAS is rapid, flexible, inexpensive and has the potential to be of centimetre scale spatial resolution (Eisenbeiss et al., 2005; Lejot et al., 2007; Vericat et al., 2009; Harwin and Lucieer 2012; Niethammer et al., 2012; Turner et al., 2012). Reported drawbacks have related primarily to the difficulties in processing imagery obtained from the relatively unstable UAS platforms using lightweight, low cost, non-metric cameras. This results in large illumination differences between images and geometric distortions introduced by off-nadir image acquisition and lack of information concerning the external flight parameters typically

required by photogrammetry (Dugdale, 2007; Lejot et al., 2007; Dunford et al., 2009; MacVicar et al., 2009; Smith et al., 2009; Laliberté et al., 2008; Vericat et al., 2009; Rosnell and Honkavaara 2012; Turner et al., 2012).

In parallel to these developments in imaging platforms, topographic surveying has been undergoing another methodological revolution with the development of Structure from Motion (SfM) photogrammetry. SfM-photogrammetry reconstructs 3D scenes by automatically matching conjugate points between images acquired from different viewpoints (Snavely et al., 2006; Snavely et al., 2008). With over 1700 publications[1], SfM-photogrammetry approaches have been a major research focus in computer vision for over a decade, but their application to the earth sciences has been slow. SfM-photogrammetry can restitute topography from suitable image datasets with minimal input of real-world ground control points. The data are produced as very dense, arbitrarily scaled 3D point clouds. Ground control and/or camera locations are only required when the user needs to transform the relative, arbitrarily scaled, elevation dataset (either a raster or a point cloud) to map coordinates with correctly scaled elevations. Whilst based on the same fundamental image geometry as traditional photogrammetry, the success of SfM-photogrammetry approaches rests on a new generation of image matching algorithms first developed three decades ago (Lucas and Kanade, 1981). Since then, image matching has become another heavily researched area with over 2600 published works[2]. SfM-photogrammetry has now been integrated into readily available software packages such as the commercial PhotoScan (Agisoft LLC), the free 123D Catch (Autocad Inc) and the open source VisualSFM (http://ccwu.me/vsfm/ by C. Wu). These software

[1] Web of Science search performed on 4th February 2014 for the exact phrase 'Structure from Motion' returned approximately 1782 papers.
[2] Web of Science search performed on 4th February 2014 for the exact phrase 'Image Matching' returned approximately 2637 papers.

packages employ a workflow which is very similar to traditional photogrammetry but with certain differences. As such this new approach to photogrammetry can be described as 'SfM-photogrammetry'.

SfM-photogrammetry has two key differences from traditional photogrammetry. Firstly, the collinearity equations are solved without prior knowledge of camera positions or ground control. Secondly, SfM-photogrammetry has the ability to match points from imagery of extremely differing scales, view angles and orientations - therefore providing significant advantages for use with UAS imagery (Rosnell and Honkavaara 2012; Turner et al., 2012; Fonstad et al., 2013).

Published examples of the use of SfM-photogrammetry for topographic assessment have only started to emerge since about 2011 but include application in the fields of archaeology (e.g. Verhoeven, 2012; Verhoeven et al., 2012) and geomorphology (e.g. James and Robson 2012; Westoby et al., 2012; Harwin and Lucieer 2012; Javernick et al., 2014). These initial studies demonstrate a technique which is rapid and largely automated and therefore easily performed by non-experts. The approach is relatively inexpensive, and capable of producing elevation datasets with mean errors in the range 0.02-0.15m, assuming the appropriate use of ground control (Harwin and Lucieer 2012; Turner et al., 2012; Verhoeven, 2012; Verhoeven et al., 2012; Westoby et al., 2012; Fonstad et al., 2013; Javernick et al., 2014).

The combined use of UAS with SfM-photogrammetry remains in its infancy and has seen very little evaluation for applications within fluvial science and management. Fonstad et al., (2013) provide the only known published example of UAS imagery processed using SfM-photogrammetry for the quantification of fluvial topography. Imagery was acquired using a helikite UAS, processed using a freeware SfM-

photogrammetry package and georeferenced to produce a point cloud for the exposed topography. The resulting point cloud density was high (10.8 points/m^2), with a mean elevation error of 0.07m and precision (standard deviation) of 0.15m.

To our knowledge no published work has yet assessed the use of a UAS-SfM approach for quantifying topography within submerged areas. As a result, we need rigorous and robust quantitative testing which compares outputs with well-established topographic surveying techniques and evaluates this approach as a tool for characterising fluvial geomorphology.

Within this research, we aim to test the use of UAS imagery processed using SfM-photogrammetry for creating hyperspatial resolution (<0.1m) topographic datasets at the mesoscale. This test will encompass both exposed and submerged parts of the fluvial environment at two different river sites. A quantitative assessment is undertaken by addressing the following research questions;

1. How accurate, precise and replicable are the topographic datasets generated?
2. How does the accuracy and precision of the datasets vary between different river systems?
3. How does the accuracy and precision of the datasets vary between exposed and submerged terrain, and does the application of a simple refraction correction procedure improve the accuracy in submerged areas?

2. Site Locations

We collected imagery from a UAS at two contrasting river locations. These sites were chosen because they provide diverse topographic conditions at the mesoscale,

within different landscape settings. Both sites feature small (<12m wide) and shallow (<0.7m deep) channels which were easily accessible. Permission from the landowners was granted for UAS flying. Neither of the sites have continuous tree coverage, nor are they near major roads or railway lines, power lines or sensitive sites such as airports - factors which might prohibit UAS flying.

The two sites are as follows;

(1) **The River Arrow**, near Studley in Warwickshire, UK (Figure 2). This lowland river is a small (c. 5-12m wide), meandering, pool-riffle system with a bed composed predominantly of cobbles with some submerged aquatic vegetation. We conducted three surveys over a 50m reach of the River Arrow in May, June and August 2013, in order to assess the repeatability of the approach. Average water depth during these surveys ranged between 0.15m and 0.18m, and maximum water depth between 0.50m and 0.57m.

(2) **Coledale Beck,** near Braithwaite in Cumbria, UK (Figure 2). This river is a small (c.3-10m wide), pool-riffle system and is gently meandering. The site features a number of exposed point bars and opposing steep, undercut banks. We collected UAS imagery of a 100m reach of Coledale Beck in July 2013. During the survey average water depth was 0.14m and maximum water depth was 0.70m within this reach.

3. Methods

Figure 3 provides an overview of our workflow, which included the following methods.

3.1 Image Acquisition

At the present time, the UK's Civil Aviation Authority (CAA) requires neither a licence nor specific permission to operate a small UAS (<7kg) for academic research purposes where one or more of the following risk mitigating factors apply; airspace segregation, visual line of sight operation and low aircraft mass (Civil Aviation Authority, 2012). Despite this, prior to conducting this research we undertook CAA approved flight training in the form of the Basic National UAS Certificate for Small UAS (BNUC-S™). We operated a Draganflyer X6 UAS with on board camera, and adhered to the conditions of the CAA permit at all times.

The Draganflyer X6 ('the X6' - Figure 4) is a small and lightweight (1kg) rotary-winged system, capable of carrying a 0.5kg payload. With the exception of an automated take-off, flight control and image acquisition are entirely manual using handheld, wireless flight controllers. The cost of the X6, including flight training, the camera and all other accessories was approximately £29,500 at the time of purchase in 2010.

Following flight training and initial flying tests, we found that a two-person team is ideal for flying the X6 and acquiring imagery. The first person is solely responsible for manual flight control and the second for navigation and manual trigger of the camera shutter for image acquisition. Navigation is conducted by eye using either specially integrated video goggles or a base station with laptop, both of which display real-time imagery from the airborne camera via radio link. We ensured sufficient site coverage by manual checking of images in between flights. Multiple flights were often required at each site, as each X6 LiPo (lithium polymer) battery provides only 3-5 minutes of flying time.

A Panasonic Lumix DMC-LX3 10.1 megapixel consumer-grade digital RGB camera is mounted on the X6 for image acquisition. The camera is wired into the control circuit of the X6, allowing the camera to be controlled remotely and to draw power from the on board LiPo battery. The original camera firmware is not altered.

Prior to image acquisition we undertook calibration of the Lumix camera by fixing targets to a flat vertical surface (the wall of a large sports hall) and photographing the targets from set distances (Figure 3 – Step 1). This allowed us to determine the relationship between focal length, distance from the targets (as a proxy for flying altitude) and image pixel size. Based on the results of this calibration, we set a target flying altitude of c.25-30m above ground level and manually set the focal length to 5mm to ensure that all imagery had a pixel size of c.1cm. The resulting images were 3648 pixels by 2736 pixels in size and image footprint size was approximately 25m x 35m (roughly equivalent to flying altitude). We acquired images with a high level of overlap (c. 80% or greater) to allow for subsequent image matching using SfM-photogrammetry software (Figure 3 – Step 2b).

The handheld controller displays the flying altitude of the X6, which we monitored throughout each flight to ensure the target height was maintained. However we note that in practice it is difficult to maintain flight altitude precisely, especially in areas of high topographic diversity.

3.2 Ground Control

Given the lack of fixed, easily identifiable features at all research sites we constructed artificial ground control points (GCPs) from 20cm x 20cm squares of 0.5mm thick black PVC pond liner (Wheaton, 2012). We spray painted two white triangles onto each to create GCP targets similar to those often used in

photogrammetry. We distributed the GCPs prior to image acquisition (Figure 3 – Step 2a) and recorded the position of each GCP using a GNSS device or total station following image acquisition (Figure 3 – Step 2c), as detailed for each site in Table 2. Figures 4 and 5 show the quantity and spatial distribution of GCPs used at each site, which varied between surveys. Following the conclusions of Vericat et al., (2009), we made efforts to ensure GCPs were located in a uniform random pattern which represented the topographic variation at each site.

3.3 Image Selection

Following image acquisition, we assessed the quality of individual images prior to further processing (Figure 3 – Step 3a). We checked images visually to remove those affected by blurring. We also used information stored within the X6 log file to exclude images which were; a) not acquired at or near nadir, in order to minimise the effect of refraction induced by oblique viewing angles, and; b) not within an acceptable altitude range (c.22-30m above ground level). Whilst SfM-photogrammetry is capable of matching images acquired at differing flying heights (i.e. at differing scales), the exclusion of images acquired outside of the specified flying height range allowed us to ensure the outputs would be of hyperspatial resolution. The logic here is that flying altitude controls image resolution, which in turn determines the density of the resulting SfM-photogrammetry point cloud and subsequently the resolution of the DEM. The point cloud density and DEM resolution is also a function of the level of image overlap. However, it is not possible to maintain a consistent level of overlap in the same way as it is to maintain flying altitude using the manually operated X6 platform and manually triggered camera.

Table 3 details the total number of images acquired at each site and the subset of these taken forward for processing. Due to the large numbers of images initially acquired, we could make these exclusions without creating gaps in image coverage.

3.4 Image Processing

We processed the imagery acquired at both sites using PhotoScan Pro version 0.9.1.1714 (Agisoft LLC). At the time of writing, this SfM-photogrammetry package is available to academic institutions under an educational licence for $549, and for $3499 for commercial use (Agisoft LLC, 2014). PhotoScan Pro contains all the necessary routines required to output rasterised DEMs, fully orthorectified imagery and dense point clouds from the raw UAS imagery. Our workflow comprised the following key steps: image import, image alignment, geometry building, texture building, georeferencing, optimisation of image alignment and re-building of scene geometry and texture (Figure 3 – Step 4).

The algorithms implemented in PhotoScan are similar to the Scale Invariant Feature Transform (SIFT) proposed by Lowe (2004), and differ from those used in standard photogrammetry. Image templates are bypassed in favour of a multiscalar, local image gradients approach. This method allows sub-pixel accuracy with invariance to scale, orientation and illumination – a key advantage for use with UAS imagery (Lowe, 2004; Snavely et al., 2006; Snavely et al., 2008). Additionally, these advanced feature matching algorithms are so computationally efficient and accurate that imagery can be uploaded in a random manner without affecting the success of the matching process. Readers are referred to recent papers by James and Robson (2012), Turner et al., (2012) and Javernick et al., (2014) for further detail on the SfM process.

The georeferencing stage is crucial for quantitative geomorphological investigations, as it allows the data to be scaled, translated and rotated to real-world co-ordinates. The XYZ positions of the GCPs were imported into PhotoScan for each dataset and used in a least-squares sense in order to derive the 7 parameters (1 scale, 3 translation and 3 rotation parameters) needed to register the model to real-world coordinates. In theory, the georeferencing process requires a minimum of 3 GCPs. In practise it is likely that more GCPs will produce a better registration, however it is not yet clear what the optimum number of GCPs is or how they should be distributed.

The georeferencing process provides a linear, affine, transformation of the model, but cannot remove non-linear model misalignments. Therefore, it is necessary to optimise the initial alignment of images following georeferencing (Figure 3 – Step 4f). In this process, known GCP co-ordinates are used to refine the camera lens model in order to minimise geometric distortions within the 3D model. As a result, reprojection errors and reference co-ordinate misalignment errors are reduced in the final output geometry (Agisoft LLC, 2013). Subsequently the model geometry is then re-built and the texture re-mapped (Figure 3 – Step 4g and 4h).

It is possible to carry out georeferencing on the sparse point cloud, prior to the first building of geometry and texture mapping. This would save processing time, but we found that accurate placement of GCP marker positions was easier on the textured model than on the initial sparse point cloud.

The outputs of this SfM-photogrammetry process include orthorectified image mosaics and DEMs for each survey, referenced to their respective UTM co-ordinate systems (Figures 5 and 6). Table 3 provides further detail concerning the spatial resolution of these products.

3.5 Refraction Correction

Within submerged areas, the SfM-photogrammetry outputs will have been affected by refraction at the air-water interface (Figure 1). Typically this results in an overestimation of the true bed elevation, as observed within studies using digital photogrammetry in submerged areas (Fryer, 1983; Fryer and Kneist 1985; Butler et al., 2002; Westaway et al., 2001). Given the acquisition of UAS imagery predominantly at nadir, here we test the use of a simple refraction correction procedure for through-water photogrammetry, as described by Westaway et al., (2000). Apparent water depths are multiplied by the refractive index of clear water to obtain refraction corrected water depths (Figure 3 – Step 5). We assess the success of this procedure by comparison to topographic validation data collected within submerged areas.

Applying this refraction correction required us to model the water surface elevation in order to estimate water depths. We mapped the position of the water's edge from each orthophoto at a scale of 1:50. At 0.25m intervals along this mapped line, we extracted DEM elevation values and interpolated between them using a TIN model, to produce estimated water surface elevations. We subtracted the underlying DEM from this surface to give estimates of water depth, as a raster dataset. Next, we multiplied the resulting depth values by 1.34 (the refractive index of clear water) to produce maps of refraction corrected water depth. This allowed us to create maps of refraction corrected submerged channel elevations by subtracting the difference in water depth between the non-corrected and corrected datasets from the original DEM. This process assumes a planar water surface, unaffected by waves or surface rippling. In reality this is very unlikely, but an assessment of the impact of surface waves on refraction is beyond the scope of this study.

3.6 Ground Validation

In order to validate the topographic data produced using the UAS-SfM approach, we collected independent elevation data using traditional topographic surveying methods (Figure 3 – Step 2d). This included the use of a differential GPS or total station across both exposed and submerged parts of each site. Table 2 shows the numbers of validation points collected at each site.

At both sites, we established 4 permanent marker positions which we surveyed in using a Trimble R8 network RTK system (River Arrow) or a Leica GPS1200 dGPS (Coledale Beck). The latter were post-processed using RINEX data. We surveyed the ground validation data relative to these markers, using a Leica Builder 500 total station. The use of permanent markers was particularly important at the River Arrow site where we conducted repeat surveys between May and August 2013. During the collection of topographic validation data we also recorded measures of water depth to the nearest centimetre.

3.7 DEM Accuracy

We conducted an additional UAS flight within a large sports hall to test the ability of the SfM-photogrammetry approach to reconstruct a flat surface. A total of 34 images were acquired at or as close to nadir as possible from the Panasonic Lumix DMC-LX3 camera on board the X6. We flew the X6 at a height of c. 4m above ground level, covering an area roughly 9m x 7m. We processed the imagery within PhotoScan Pro to produce an orthophoto and DEM (Figure 7), as described earlier, and performed georeferencing using 7 GCPs. The GCPs were evenly distributed within the scene, and surveyed into a local co-ordinate system using a Leica Builder

500 total station. We also used the total station to collect 30 validation points to check for elevation variation within the supposedly 'flat' surface.

4. Results

Table 3 provides an overview of the data coverage and resolution by site, and the time taken for data collection and processing. First, we conducted a quantitative assessment of the topographic data produced from the UAS-SfM process by comparison against the independent ground validation data for each site. We assessed both the original DEM and the refraction corrected DEM by calculating the elevation mean error (accuracy) and standard deviation (precision), and by performing regression against the independent validation data. Table 4 and Figures 8 to 10 present the results.

Second, we calculated residual errors in the planimetric (X, Y) and the vertical (Z) by comparing the measured positions of all GCPs against their mapped positions on the orthophoto and DEM (Table 5). The mean of X, Y residual errors at all sites is almost always less than 0.01m. This is less than the pixel size of the DEMs, thereby suggesting the residual planimetric error will have minimal impact on the independent validation of the topographic data. Larger residual errors occur in some places, as indicated by the standard deviation values also given in Table 5. In some cases, these values exceed the pixel size (0.02m) and therefore may start to affect the validation of DEM accuracy in Z.

4.1 Exposed Areas

For exposed areas, DEM accuracy is highest for the datasets acquired at the River Arrow where mean error ranges are consistently low, i.e. between 0.004m and

0.04m (Table 4). The equivalent values at Coledale Beck are slightly worse (0.11m) and relate to the presence of tall, dense bracken and grasses covering much of this site. The removal of validation points collected in such areas leads to an improvement in mean error to -0.04m.

Table 4 presents a similar pattern of DEM quality for exposed areas as observed from the standard deviation values. DEM precision is highest for the River Arrow datasets (c. 0.02-0.07m), and considerably poorer at Coledale Beck (0.2m). Again, the value for Coledale can be improved (to 0.08m) by exclusion of points in areas of tall vegetation.

The strength of the relationship between the DEM and independent validation data is indicated by the regressions presented in Figure 8. High R^2 values (>0.98) are returned for all sites, with the River Arrow datasets displaying the strongest values (all >0.99). Within the regression line equations, slope values closest to 1 and intercept values closest to 0 represent the best match between the DEM and corresponding independent validation data. Again, the best results are observed within the River Arrow datasets (Figure 8a-c), with poorer results from Coledale Beck (Figure 8d).

4.2 Submerged Areas – No Correction

Table 4 shows that DEM quality (as expressed by the mean error and standard deviation values) is nearly always poorer in submerged areas than in exposed areas. The lowest mean error of 0.017m is observed for Coledale Beck, and low values are also found for the River Arrow datasets (0.053-0.089m). The values of precision for the Coledale and Arrow datasets are similar, in the range of 0.06-0.08m. The Arrow datasets show a reduced strength of correlation for submerged areas (compared to

the datasets for exposed areas), with R^2 values within the range 0.78-0.88 (Figure 9a-c). The co-efficient of determination for the Coledale data is improved very slightly from 0.98 in exposed areas to 0.99 in the submerged zone (Figure 9d).

4.3 Water Depth and DEM Error

Figure 10 shows the correlation between water depth and DEM error for all sites. These are independent measures of water depth, acquired in the field to the nearest centimetre. For all surveys DEM error appears to increase with water depth (thereby demonstrating the probable effects of refraction). This trend is strongest for the Arrow datasets, with R^2 values at about 0.50, and slightly less strong for the Coledale data ($R^2 = 0.40$).

4.4 Submerged Areas – With Refraction Correction

Figure 11 provides two example cross sections, demonstrating the effect of the refraction correction on the DEM in submerged areas. Table 4 and Figure 9 suggest that the effect of the refraction correction procedure on DEM quality in submerged areas is variable. Mean error is found to be consistently improved for all datasets collected at the River Arrow (by c. 0.03-0.06m), but the same is not observed for Coledale where mean error is worsened. There is no significant change in DEM precision or strength of the correlation for any of the surveys. However, the nature of the relationship between the DEM and validation data (as indicated by the regression line equations) is improved in all cases. That is, the slope is closer to 1 and the intercept closer to 0.

We re-calculated DEM error following refraction correction and re-plotted this against water depth for all surveys. As shown in Figure 10, this has the effect of reducing the depth dependency of the error for all datasets at both sites.

4.5. Spatial patterns of DEM quality

In theory, the DEM of the sports hall floor should be flat. Statistically, this DEM had a mean error of 0.005m and a standard deviation of 0.005m. However, we constructed a simple cross section of the DEM (Figure 12a) which shows a dome-like deformation with a central peak which is c. 0.02m above the surface and edges which are c. 0.02m below the surface. In addition to the deformation, small-scale noise with an amplitude of c. 0.002m was present.

For the river reaches, Figures 12b and 12c shows the errors plotted spatially. In the Coledale reach (Figure 12c), we also see a dome-like deformation with larger underpredictions at the edge of the DEM. In this case, the amplitude of the dome-like deformation is c. 0.2m. However, Figure 12b does not suggest any pattern in the error distribution.

5. Discussion

5.1 Exposed Areas

The quantitative assessment of the UAS-SfM approach used at the River Arrow and Coledale Beck sites has demonstrated the ability to produce hyperspatial (c. 0.02m), continuous topographic datasets for exposed parts of the fluvial environment, with high levels of accuracy (0.004-0.04m) and precision (0.02-0.07m) for areas which are non-vegetated or feature only low-level vegetation (such as short grass). These results are comparable with existing findings in the use of UAS and SfM-

photogrammetry for quantifying topography in both fluvial and other settings (Lejot et al., 2007; Harwin and Lucieer 2012; James and Robson 2012; Fonstad et al., 2013), and are approaching those possible with TLS for exposed areas (Heritage and Hetherington 2007; Milan et al., 2010; Bangen et al., 2013).

Table 4 presents ratios for *precision: flying height* and *pixel size: precision*. These ratios give an indication of the magnitude of error in relation to flying altitude and pixel size (or DEM resolution). In exposed areas, the *pixel size: precision* ratios indicate that mean error varies from less than the pixel size (Arrow May and June datasets) to more than five times the pixel size (Coledale). The *precision: flying height* ratios range from 1: 257 (where vegetation degrades mean error) to as high as c. 1: 6613. According to the recent research of James and Robson (2012), *precision: flying height* ratios previously obtained using SfM-photogrammetry for surface reconstruction from an aerial survey are in the region 1: 1000-1800, and theoretical estimates from conventional photogrammetry using metric cameras are in the range 1: 1080-9400. The results we have obtained suggest the UAS-SfM approach is providing *precision: flying height* ratios at best in line with those obtained from traditional photogrammetry, and sometimes below. We suspect that the lower *precision: flying height* ratios obtained for the River Arrow August and Coledale datasets relate to the presence of taller and denser vegetation at these sites during image acquisition campaigns which were conducted later in the summer.

The three surveys conducted at the River Arrow indicate that the UAS-SfM approach is repeatable and objective, consistently producing high quality orthophotos and DEMs for exposed areas with low mean errors in comparison with the independent validation data (Table 4), and low residual errors in X, Y and Z associated with georeferencing (Table 5).

5.2 Submerged Areas and Refraction Correction

High resolution topographic data are also available for the submerged parts of both sites. Table 4 indicates slightly reduced levels of accuracy (0.02-0.09m) and precision (0.06-0.09m), and lower *precision: flying height* and *pixel size: precision* ratios compared to exposed areas. All datasets show that the DEM consistently over-predicts elevation, a trend which appears to increase with water depth (Figure 10). This suggests that the DEM error in submerged areas is depth dependent. Similar studies using through-water digital photogrammetry have found comparable results and have attributed this overestimation to a combination of refraction effects and the photogrammetric process fixing matches at points within the water column, but above the channel bed (Tewinkel, 1963; Fryer, 1983; Fryer and Kniest 1985, Westaway et al., 2000; Westaway et al., 2001; Butler et al., 2002; Feurer et al., 2008). Furthermore, the use of 8-bit imagery displaying radiation intensities in 256 grey levels reduces contrast (or texture) in the deeper, darker parts of the scene. This reduction in radiometric resolution has been found to reduce the success of optical bathymetric mapping (Legleiter et al., 2004; Legleiter, 2013). We assume that the reduced image texture in deeper parts of the channel may also adversely affect the success of the SfM-photogrammetry matching process in these areas, and therefore also affect the DEM accuracy.

The application of the simple refraction correction procedure has the effect of reducing DEM errors by c. 50%, as indicated by the *pixel size: precision* ratios in Table 4. Mean error values are also significantly improved following refraction correction (i.e. reduced overestimation by the DEM - Figure 9a-c), where there is an existing correlation between error and water depth (Figure 10a-c). These improvements are not observed for the Coledale dataset, perhaps because the

correlation between DEM error and water depth is weaker for Coledale (Figure 10d) and mean error is already very low prior to refraction correction (0.017m). In fact, this mean error value is already comparable to that obtained for exposed areas and perhaps suggests that refraction correction is not required. The work of Westaway et al., (2001) using through-water digital photogrammetry reports that at water depths less than 0.2m, the effects of refraction are negligible thereby deeming correction procedures unnecessary. Coledale Beck is a very shallow stream and has the highest percentage of validation points which fall within depths of less than or equal to 0.2m (83%). Therefore, we suggest that this is why the refraction correction procedure has limited effect at this site. Further research specifically testing this hypothesis is required to confirm this.

Whilst the effect on mean error differs between the Arrow and Coledale datasets, refraction correction has the effect of reducing the magnitude of overestimation with depth at both sites, but does not entirely eliminate it (Figure 10). This may result from the SfM-photogrammetry process matching points within the water column at elevations higher than the channel bed, as found in similar photogrammetry studies (Westaway et al., 2001).

The repeat surveys at the River Arrow site confirm the repeatability of the approach for submerged areas. Whilst the most accurate and precise results are obtained for the June 2013 dataset, all surveys produce DEMs with both a mean error and standard deviation less than 0.09m prior to refraction correction (Table 4). Furthermore, the refraction correction procedure has the effect of improving the accuracy of the DEM to less than 0.06m in submerged areas for all River Arrow surveys.

With reference to Table 1, it is clear that for DEMs produced in submerged areas using the UAS-SfM approach (with refraction correction) provide finer resolution datasets (0.02m) with lower mean errors (0.004-0.06m) than those reported for bathymetric laser scanning, digital photogrammetry and the spectral-depth method. However, these approaches are often conducted at quite different scales. TLS surveys are more comparable to the UAS-SfM approach in terms of scale of assessment. Our results demonstrate that the UAS-SfM approach is capable of providing data resolutions exceeding those reported for TLS at the mesoscale in submerged areas, with similar accuracies and reduced data collection times (Smith and Vericat, 2013).

The UAS-SfM approach is capable of returning topographic data in areas as deep as 0.7m in clear water and with adequate illumination. However, refraction correction is needed, and the technique performs best at depths less than 0.2m. This is roughly in line with maximum water depths achieved by digital photogrammetry and TLS, but is shallower than that achieved using bathymetric LiDAR and the spectral-depth approach (Table 1).

5.3 Evaluation of the UAS-SfM Approach for Fluvial Topography

Ultimately, the choice of a method for quantifying topography, within both fluvial and other settings, will be determined by the specific requirements of the intended application in terms of scale and accuracy, as well as the availability of resources, time and funds. Within this paper we have demonstrated the potential of a UAS-SfM approach for quantifying the topography of fluvial environments at the mesoscale with hyperspatial resolutions (0.02m). This approach provides a single surveying technique for generating accurate and precise DEMs for non-vegetated exposed

areas of the fluvial environment, and within submerged areas for depths up to 0.7m providing the water is clear, there is limited water surface roughness (e.g. white water) and refraction correction is implemented. As such, it represents an important innovation over hybrid approaches and has potential as a tool for characterising topographic heterogeneity at the mesoscale within a 'riverscape' style framework (Fausch et al., 2002).

Platform mobilisation and data collection are relatively rapid using the Draganflyer X6 UAS. With a skilled UAS pilot and low wind speeds (ideally <2.24 metres per second), imagery covering c. 200m lengths of channel of widths of up to c. 40m can easily be obtained within day's fieldwork by a team of two people, including setup and surveying of GCPs. Processing times within PhotoScan are also relatively fast, as indicated in Table 3.

Errors within the point clouds and DEMs produced using SfM-photogrammetry remain a key concern however. In the case of PhotoScan, the 'black box' nature of the interface means that exact sources of error are almost impossible to isolate. In traditional photogrammetry, it has been established that the self-calibration of camera lens models is error prone in image datasets acquired at nadir from consumer grade digital cameras (Wackrow and Chandler, 2008). Furthermore, Wackrow and Chandler (2011) have demonstrated that images acquired at nadir produce dome-like deformations as we have observed in Figures 12a and 12c. Javernick et al., (2014), also find a dome-like pattern of error before the optimisation of the lens model in PhotoScan. However, this dome-like deformation is not reported by Westoby et al., (2012) or Fonstad et al., (2013). Our results show that the amplitude of this dome-like deformation is moderate. It appears to scale with flying height, with *amplitude: flying height* ratios of 1:200 and 1:300 for the cases of the

indoor and outdoor flights respectively. In absolute terms, these errors can be deceptively small for small flying heights and may have gone unreported in previous literature. Wackrow and Chandler (2011) find that the addition of oblique imagery with convergent view-angles eliminates the dome-like deformation. It is therefore possible that the dome-like deformation is not present for image acquisitions with sufficient variability around nadir. At the very least, it would seem that greater consideration must be given to image viewing angle during the flight planning phase, when consumer grade digital cameras are being used (Wackrow and Chandler, 2011). However, in the present case and with respect to the objective of submerged topography mapping, oblique imagery would be affected differently by refraction and therefore the combined usage of nadir and oblique imagery could require a more advanced refraction correction procedure. Further research is clearly needed if we are to understand error sources in SfM-photogrammetry and potential users should be aware that the visually stunning outputs are by no means error-free.

6. Conclusions and Future Work

Within this study we have provided a quantitative assessment of the use of high resolution UAS imagery, processed within an SfM-photogrammetry workflow, to generate topographic datasets for both the exposed and submerged parts of two different river systems. Within exposed areas, the topographic outputs are of hyperspatial resolution (0.02m), with accuracy and precision values approaching those typically obtained using TLS. DEM accuracy and precision were slightly poorer within submerged areas, with an apparent scaling of error with increasing water depth. A simple refraction correction procedure improved results in submerged areas for sites where there was an existing correlation between error and water depth. Multiple surveys acquired from the River Arrow site gave consistently high quality

results, indicating the repeatability of the approach. However, we have observed a dome-like deformation which can be present in SfM-photogrammetry DEMs. This deformation can be small in absolute terms and users of SfM-photogrammetry should be cautious about using the resulting DEMs in process models that are sensitive to slope. Key areas which would benefit from further targeted research include; the effects of varying camera orientation during image acquisition; the effects of varying GCP densities; the effects of varying the level of image overlap; the potential of alternative refraction correction procedures; direct comparisons with TLS data in submerged environments; and the ability of repeat surveys for detecting geomorphic change. This UAS-SfM technique has potential as a valuable tool for creating high resolution, high accuracy topographic datasets for assessment of fluvial environments at the mesoscale and a wide range of other geomorphological applications.

7. Acknowledgements

This work was carried out as part of a University of Worcester funded PhD studentship. We thank the British Society for Geomorphology and the Geological Remote Sensing Group for providing postgraduate funding awards to Amy Woodget and Bath Spa University for additional financial support. The fieldwork assistance of James Atkins, Robbie Austrums, Milo Creasey, Rich Johnson, Jenni Lodwick, Jeff Warburton, William Woodget and others at the Universities of Worcester and Bath Spa is gratefully acknowledged. We also thank Carl Legleiter and one anonymous reviewer for constructive review comments.

8. References

Agisoft LLC. 2013. Agisoft PhotoScan User Manual: Professional Edition, Version 1.0.0.

Bailly, J-S., Le Coarer, Y., Languille, P., Stigermark, C. and Allouis, T. 2010. Geostatistical estimation of bathymetric LiDAR errors on rivers. *Earth Surface Processes and Landforms* 35: 1199-1210

Bailly, J-S., Kinzel, P.J., Allouis, T., Feurer, D. and Le Coarer, Y. 2012. Airborne LiDAR methods applied to riverine environments. In *Fluvial Remote Sensing for Science and Management,* Carbonneau, P.E. and Piegay, H. (eds). Wiley-Blackwell, Chichester

Bangen, S.G., Wheaton, J.M., Bouwes, N., Bouwes, B. and Jordan, C. 2013. A methodological intercomparison of topographic surveying techniques for characterizing wadeable streams and rivers. *Geomorphology* doi:10.1016/j.geomorph.2013.10.010

Bergeron, N. and Carbonneau, P.E. 2012. Geosalar: Innovative remote sensing methods for spatially continuous mapping of fluvial habitat at riverscape scale' In *Fluvial Remote Sensing for Science and Management,* Carbonneau, P.E. and Piegay, H. (eds). Wiley-Blackwell, Chichester

Butler, J.B., Lane, S.N. and Chandler, J.H. 2001. Automated extraction of grain-size data from gravel surfaces using digital image processing. *Journal of Hydraulic Research* 39 (5): 519-529

Butler, J.B., Lane, S.N., Chandler, J.H. and Porfiri, E. 2002. Through-water close range digital photogrammetry in flume and field environments. *Photogrammetric Record* 17 (99): 419-439

Carbonneau, P.E., Lane, S.N. and Bergeron, N. 2003. Cost-effective non-metric close-range digital photogrammetry and its application to a study of coarse gravel river beds. *International Journal of Remote Sensing* 24: 2837-2854

Carbonneau, P.E., Lane, S.N. and Bergeron, N. 2006. Feature based image processing methods applied to bathymetric measurements from airborne remote sensing in fluvial environments. *Earth Surface Processes and Landforms* 31: 1413-1423

Carbonneau, P.E., Fonstad, M.A., Marcus, W.A. and Dugdale, S.J. 2012. Making riverscapes real. *Geomorphology* 123: 74-86

Civil Aviation Authority. 2012. CAP 722 – Unmanned Aircraft System Operations in UK Airspace – Guidance (www.caa.co.uk, accessed 25.02.2014).

Dugdale, S.J. 2007. An evaluation of imagery from an unmanned aerial vehicle (UAV) for the mapping of intertidal macroalgae on Seal Sands, Tees Estuary, UK. Unpublished MSc thesis, Durham University

Dunford, R., Michel, K., Gagnage, M., Piegay, H. and Tremelo, M-L. 2009. Potential constraints of unmanned aerial vehicle technology for the characterization of Mediterranean riparian forest. *International Journal of Remote Sensing* 30 (19): 4915-4935

Eisenbeiss, H., Lambers, K., Sauerbier, M. and Li, Z. 2005. Photogrammetric documentation of an archaeological site (Palpa, Peru) using an autonomous model helicopter. *CIPA 2005 XX International Symposium,* 26 September-1 October, Torino, Italy

Fausch, K.D., Torgersen, C.E., Baxter, C.V. and Hiram, L.W. 2002. Landscapes to riverscapes: bridging the gap between research and conservation of stream fishes. *BioScience* 52 (6): 483-498

Fernandez, D., Barquin, J. and Raven, P. 2011. A review of river habitat characterisation methods: indices vs. characterisation protocols. *Limnetica* 30 (2): 217-234

Feurer, D., Bailly, J-S., Puech, C., Le Coarer, Y. and Viau, A.A. 2008. Very-high-resolution mapping of river-immersed topography by remote sensing. *Progress in Physical Geography* 32(4): 403-419

Fonstad, M.A., Dietrich, J.T., Courville, B.C., Jensen, J.L. and Carbonneau, P.E. 2013. Topographic structure from motion: a new development in photogrammetric measurement. *Earth Surface Processes and Landforms* doi: 10.1002/esp.3366

Frissell, C.A., Liss, W.J., Warren, C.E. and Hurley, M.D. 1986. A hierarchical framework for stream habitat classification: viewing streams in a watershed context. *Environmental Management* 10 (2): 199-214

Frothingham, K.M., Rhoads, B.L. and Herricks, E.E. 2002. A multiscale conceptual framework for integrated ecogeomorphological research to support stream naturalisation in the agricultural Midwest. *Environmental Management* 29 (1): 16-33

Fryer, J.G. 1983. A simple system for photogrammetric mapping in shallow water. *Photogrammetric Record* 11 (62): 203-208

Fryer, J.G. and Kniest, H.T. 1985. Errors in depth determination caused by waves in through-water photogrammetry. *Photogrammetric Record* 11 (66): 745-753

Harwin, S. and Lucieer, A. 2012. Assessing the accuracy of georeferenced point clouds produced via multi-view stereopsis from unmanned aerial vehicle (UAV) imagery. *Remote Sensing* 4: 1573-1599

Heritage, G. and Hetherington, D. 2007. Towards a protocol for laser scanning in fluvial geomorphology. *Earth Surface Processes and Landforms* 32: 66-74

Hervouet, A., Dunford, R., Piegay, H., Belletti, B. and Tremelo, M-L. 2011. Analysis of post-flood recruitment patterns in braided-channel rivers at multiple scales based

on an image series collected by unmanned aerial vehicles, ultra-light aerial vehicles, and satellites. *GIScience and Remote Sensing* 48 (1): 50-73

Hicks, D.M. 2012. Remotely sensed topographic change in gravel riverbeds with flowing channels. In *Gravel-bed Rivers: Processes, Tools, Environments*, Church, M., Biron, P. and Roy, A. (Eds) Wiley-Blackwell, Chichester

Hugenholtz, C., Whitehead, K., Brown, O.W., Barchyn, T.E., Moorman, B.J., LeClair, A., Riddell, K., and Hamilton, T. 2013. Geomorphological mapping with a small unmanned aircraft system (sUAS): Feature detection and accuracy assessment of a photogrammetrically derived digital terrain model. *Geomorphology* 194: 16-24

James, M.R. and Robson, S. 2012. Straightforward reconstruction of 3D surfaces and topography with a camera: accuracy and geoscience application. *Journal of Geophysical Research* 117, F03017, doi: 10.1029/2011JF002289

Javernick, L., Brasington, J. and Caruso, B. 2014. Modelling the topography of shallow braided rivers using Structure-from-Motion photogrammetry. *Geomorphology* doi: 10.1016/j.geomorph.2014.01.006

Jerlov, N.G. 1976. Marine Optics. Elsevier, Amsterdam.

Kinzel, P.J., Wright, C.W., Nelson, J.M. and Burman, A.R. 2007. Evaluation of an experimental LiDAR for surveying a shallow, sand-bedded river. *Journal of Hydraulic Engineering* 133 (7): 838-842

Kinzel, P.J., Legleiter, C.J. and Nelson, J.M. 2013. Mapping river bathymetry with a small footprint green lidar: applications and challenges. *Journal of the American Water Resources Association* 49 (1): 183-204

Laliberté, A.S., Winters, C. and Rango, A. 2008. A procedure for orthorectification of sub-decimeter resolution imagery obtained with an unmanned aerial vehicle (UAV). *Proceedings of the American Society for Photogrammetry and Remote Sensing Annual Conference*, Portland, Oregon, 28 April-2 May 2008.

Lane, S.N. 2000. The measurement of river channel morphology using digital photogrammetry. *Photogrammetric Record* 16 (96): 937-957

Lane, S.N. and Carbonneau, P.E. 2007. High resolution remote sensing for understanding instream habitat' in *Hydroecology and Ecohydrology*, Wood, P.J., Hannah, D.M. and Sadler, J.P. (Eds), John Wiley and Sons, Chichester

Lane, S.N., Widdison, P.E., Thomas, R.E., Ashworth, P.J., Best, J.L., Lunt, I.A., Sambrook Smith, G.H. and Simpson, C.J., 2010. Quantification of braided river channel change using archival digital image analysis. *Earth Surface Processes and Landforms* 35(8), 971-985

Lapointe, M. 2012. River geomorphology and salmonid habitat: some examples illustrating their complex association, from redd to riverscape scales. In *Gravel-bed*

Rivers: Processes, Tools, Environments, Church, M., Biron, P. and Roy, A. (Eds) Wiley-Blackwell, Chichester

Legleiter, C.J., Roberts, D.A., Marcus, W.A. and Fonstad, M.A. 2004. Passive optical remote sensing of river channel morphology and in-stream habitat: Physical basis and feasibility. *Remote Sensing of Environment* 93: 493-510

Legleiter, C.J., Roberts, D.A. and Lawrence, R.L. 2009. Spectrally based remote sensing of river bathymetry. *Earth Surface Processes and Landforms* 34: 1039-1059

Legleiter, C.J. 2012. Remote measurement of river morphology via fusion of LiDAR topography and spectrally based bathymetry. *Earth Surface Processes and Landforms* 37: 499-518

Legleiter, C.J. 2013. Mapping river depth from publicly available aerial images. *River Research and Applications* 29 (6): 760-780

Legleiter, C.J. 2014a. A geostatistical framework for quantifying reach scale spatial structure of river morphology: 1. Variogram models, related metrics and relation to channel form. *Geomorphology* 205: 65-84

Legleiter, C.J. 2014b. A geostatistical framework for quantifying reach scale spatial structure of river morphology: 2. Application to restored and natural channels. *Geomorphology* 205: 85-101

Lejot, J., Delacourt, C., Piegay, H., Fournier, T., Tremelo, M-L. and Allemand, P. 2007. Very high spatial resolution imagery for channel bathymetry and topography from an unmanned mapping controlled platform. *Earth Surface Processes and Landforms* 32: 1705-1725

Lowe, D.G. 2004. Distinctive image features from scale-invariant keypoints. *International Journal of Computer Vision* 60: 91-110

Lucas, B.D. and Kanade, T. 1981. An iterative image registration technique with an application to stereo vision. *Proceedings of the Imaging Understanding Workshop* pp. 121-130

MacVicar, B.J., Piégay, H., Anderson, A., Oberlin, C., Comiti, F. and Pecorari, E. 2009. Quantifying the temporal dynamics of wood in large rivers: new techniques for wood tracking, monitoring, surveying, and dating. *Earth Surface Processes and Landforms* 34: 2031–2046

Maddock, I. 1999. The importance of physical habitat assessment for evaluating river health. *Freshwater Biology* 41: 373-391

Marcus, W.A. 2012. Remote sensing of the hydraulic environment in gravel-bed rivers. In *Gravel-bed Rivers: Processes, Tools, Environments*, Church, M., Biron, P. and Roy, A. (Eds) Wiley-Blackwell, Chichester

Marcus, W.A., Fonstad, M.A. and Legleiter, C.J. 2012. Management applications of optical remote sensing in the active river channel. In *Fluvial Remote Sensing for Science and Management,* Carbonneau, P.E. and Piegay, H. (Eds) Wiley-Blackwell, Chichester

Mertes, L.A.K. 2002. Remote sensing of riverine landscapes. *Freshwater Biology* 47: 799-816

Milan, D.J., Heritage, G.L., Large, A.R.G. and Entwhistle, N.S. 2010. Mapping hydraulic biotopes using terrestrial laser scan data of water surface properties. *Earth Surface Processes and Landforms* 35: 918-931

Niethammer, U., James, M.R., Rothmund, S., Travelletti, J. and Joswig, M. 2012. UAV-based remote sensing of the Super-Suaze landslide: Evaluation and results. *Engineering Geology* 128: 2-11

Nestler, J.M., Baigun, C. and Maddock, I. 2013. Achieving the aquatic ecosystem perspective: Interdisciplinary integration describes instream ecohydraulic processes' in *Ecohydraulics: An Integrated Approach.* Maddock, I., Harby, A., Kemp, P. and Wood, P. (Eds), Wiley

Newson, M.D. and Newson, C.L. 2000. Geomorphology, ecology and river channel habitat: mesoscale approaches to basin-scale challenges. *Progress in Physical Geography* 24 (2): 195-217

Orr, H.G., Large, A.R.G., Newson, M.D. and Walsh, C.L. 2008. A predictive typology for characterising hydromorphology. *Geomorphology* 100: 32-40

Rosnell, T. and Honkavaara, E. 2012. Point cloud generation from aerial image data acquired by a quadrocopter type micro unmanned aerial vehicle and a digital still camera. *Sensors* 12: 453-480

Smith, M.J., Chandler, J. and Rose, J. 2009. High spatial resolution data acquisition for the geosciences: kite aerial photography. *Earth Surface Processes and Landforms* 34: 155-161

Smith, M., Vericat, D. and Gibbins, S. 2012. Through-water terrestrial laser scanning of gravel beds at the patch scale. *Earth Surface Processes and Landforms* 37: 411-421

Smith, M.W. and Vericat, D. 2013. Evaluating shallow-water bathymetry from through-water terrestrial laser scanning under a range of hydraulic and physical water quality conditions. *River Research and Applications* (doi: 10.1002/rra.2687)

Snavely, N., Seitz, S.M. and Szeliski, R. 2006. Photo tourism: exploring photo collections in 3D. *ACM Transactions on* Graphics 25 (3): 835-846

Snavely, N., Seitz, S.M. and Szeliski, R. 2008. Modelling the world from internet photo collections. *International Journal of Computer Vision* 80 (12): 189-210

Tewinkel, G.C. 1963. Water depths from aerial photographs. *Photogrammetric Engineering* 29 (6): 1037-1042

Turner, D., Lucieer, A. and Watson, C. 2012. An automated technique for generating georectified mosaics from ultra-high resolution unmanned aerial vehicle (UAV) imagery, based on Structure from Motion (SfM) point clouds. *Remote Sensing* 4: 1392-1410

Vannote, R.L., Minshall, G.W., Cummins, K.W., Sedell, J.R. and Cushing, C.E. 1980. 'The River Continuum Concept. *Canadian Journal of Fisheries and Aquatic Science* 37: 130-137

Verhoeven, G. 2012. Getting computer vision airborne – using Structure from Motion for accurate orthophoto production. *RSPSoc Archaeology Special Interest Group Meeting Spring 2012*, p. 4-6

Verhoeven, G., Doneus, M., Briese, Ch. and Vermuelen, F. 2012. Mapping by matching: a computer vision-based approach to fast and accurate georeferencing of archaeological aerial photographs. *Journal of Archaeological Science* 39: 2060-2070

Vericat, D., Brasington, J., Wheaton, J. and Cowie, M. 2009. Accuracy assessment of aerial photographs acquired using lighter-than-air blimps: low-cost tools for mapping river corridors. *River Research and Applications* 25 (8): 985-1000

Wackrow, R. and Chandler, J.H. 2008. A convergent image configuration for DEM extraction that minimises the systematic effects caused by an inaccurate lens model. *Photogrammetric Record* 23 (121): 6-18

Wackrow, R. and Chandler, J.H. 2011. Minimising systematic error surfaces in digital elevation models using oblique convergent imagery. *Photogrammetric Record* 26 (133): 16-31

Ward, J.V. 1998. Riverine landscapes: Biodiversity patterns, disturbance regimes, and aquatic conservation. *Biological Conservation* 83 (3): 269-278

Ward, J.V., Malard, F. and Tockner, K. 2002. Landscape ecology: a framework for integrating pattern and process in river corridors. *Landscape Ecology* 17 (1): 35-45

Westaway, R.M., Lane, S.N. and Hicks, D.M. 2000. The development of an automated correction procedure for digital photogrammetry for the study of wide, shallow, gravel-bed rivers. *Earth Surface Processes and Landforms* 25: 209-226

Westaway, R.M., Lane, S.N. and Hicks, D.M. 2001. Remote sensing of clear-water, shallow, gravel-bed rivers using digital photogrammetry. *Photogrammetric Engineering and Remote Sensing* 67 (11): 1271-1281

Westaway, R.M., Lane, S.N. and Hicks, D.M. 2003. Remote survey of large-scale braided, gravel-bed rivers using digital photogrammetry and image analysis. *International Journal of Remote Sensing* 24 (4): 795-815

Westoby, M.J., Brasington, J., Glasser, N.F., Hambrey, M.J. and Reynolds, J.M. 2012. Structure-from-Motion photogrammetry: a low cost, effective tool for geoscience applications. *Geomorphology* doi.org/10.1016/j.geomorph.2012.08.021

Wheaton, J.M., Brasington, J., Darby, S.E. and Sear, D.A. 2010. Accounting for uncertainty in DEMs from repeat topographic surveys: improved sediment budgets. *Earth Surface Processes and Landforms* 35 (2): 136-156

Wheaton, J.M. 2012. http://www.joewheaton.org accessed January 2012

Wiens, J.A. 2002. Riverine landscapes: taking landscape ecology into the water. *Freshwater Biology* 47: 501-515

Williams, R.D., Brasington, J., Vericat, D. and Hicks, D.M. 2013. Hyperscale terrain modelling of braided rivers: fusing mobile terrestrial laser scanning and optical bathymetric mapping. *Earth Surface Processes and Landforms*. doi: 10.1022/esp.3437

Winterbottom, S.J. and Gilvear, D.J. 1997. Quantification of channel bed morphology in gravel-bed rivers using airborne multispectral imagery and aerial photography. *Regulated Rivers: Research and Management* 13: 489-499

Tables

Table 1. Comparison of topographic products obtained using remote sensing techniques during field tests. Values for submerged areas are shown in italics.

Approach	Typical mean error (m)	Typical spatial resolution (m)	Typical mean water depth (m)	Typical max. water depth (m)	References
Spectral-depth relationship	*0.10*	*0.05 – 4.00*	*<1.00*	*1.00*	Winterbottom and Gilvear, 1997; Westaway et al., 2003; Carbonneau et al., 2006; Lejot et al., 2007; Legleiter, 2012, 2013
Digital photo-grammetry	0.05-0.17 *0.10*	0.05 – 1.00 *0.09*	N/a *<0.60*	N/a *0.60*	Westaway et al., 2001; Westaway et al., 2003; Lejot et al., 2007; Feurer et al., 2008; Lane et al., 2010
Bathymetric LiDAR	*0.10-0.30*	*1.00*	*<1.00*	*3.90*	Kinzel et al., 2007; Feurer et al., 2008; Bailly et al., 2010, 2012
TLS	0.004-0.03 *0.01-0.10*	<0.05 *1.00*	N/a *0.10*	N/a *0.50*	Heritage and Hetherington 2007; Bangen et al., 2013; Smith and Vericat, 2013

Table 2. Data collection information by site.

Site Location	River Arrow			Coledale Beck
Date of data acquisition	May 2013	June 2013	Aug 2013	July 2013
Average flying height (m above ground level)	26.89	25.81	27.53	28.39
Number of GCPs used	21	22	16	25
Instrument used to record GCP positions	Leica Builder 500 (total station)	Leica Builder 500 (total station	Trimble R8 GNSS (RTK GPS)	Leica Builder 500 (total station
Co-ordinate System	OSGB 1936 (British National Grid)			
Number of validation points collected in exposed areas	279	218	57	532
Number of validation points collected in submerged areas	169	142	113	252

Table 3. Specification of data outputs by site.

Site Location	River Arrow			Coledale Beck
Date of data acquisition	May 2013	June 2013	Aug 2013	July 2013
Spatial coverage (m^2)	2803.50	2563.90	2084.20	4382.00
Exposed areas as % of total coverage	83.65	84.18	83.95	90.57
Submerged areas as % of total coverage	16.35	15.82	16.05	9.43
Total number of images collected	93	69	70	88
Number of images used in SfM	58	41	32	64
Spatial resolution of output orthophoto (m)	0.009	0.009	0.009	0.010
Spatial resolution of output DEM (m)	0.018	0.018	0.019	0.020
Time required in the field for set-up and image acquisition (including use of GCPs)	0.5 days	0.5 days	0.5 days	0.5 days
Time required in the field for collection of validation data	1 day	1 day	1 day	2 days
Time required for SfM image processing	0.5 days	0.5 days	0.5 days	0.5 days

*Table 4. Comparison of elevation validation observations with UAS-SfM DEM elevations. NC denotes non-corrected and RC denotes refraction corrected datasets.*Precision: Flying height ratios are calculated by dividing average flying height by mean error.**Pixel size: Precision ratios are calculated by dividing mean error by final DEM resolution (Table 3).*

Site Location		**River Arrow**			**Coledale Beck**
Date of data acquisition		May 2013	June 2013	Aug 2013	July 2013
Mean error (m)	Exposed	0.005	0.004	0.044	0.111
	Submerged (NC)	0.089	0.053	0.064	0.016
	Submerged (RC)	0.053	-0.008	0.023	-0.029
Standard deviation (m)	Exposed	0.019	0.032	0.069	0.203
	Submerged (NC)	0.073	0.065	0.085	0.078
	Submerged (RC)	0.069	0.064	0.086	0.078
Precision: Flying Height Ratio*	Exposed	1: 5119	1: 6613	1: 627	1: 257
	Submerged (NC)	1: 303	1: 484	1: 433	1: 1729
	Submerged (RC)	1: 508	1: 2991	1: 1199	1: 988
Pixel size: Precision Ratio**	Exposed	1: 0.28	1: 0.22	1: 2.32	1: 5.55
	Submerged (NC)	1: 4.94	1: 2.94	1: 3.37	1: 0.80
	Submerged (RC)	1: 2.94	1: 0.44	1: 1.21	1: 1.45

Table 5. Residual errors associated with the georeferencing of each dataset.

Site Location		River Arrow			Coledale Beck
Date of image acquisition		May 2013	June 2013	August 2013	July 2013
Mean of residual errors (m)	X	0.006	-0.028	0.007	0.006
	Y	-0.001	0.008	0.007	-0.007
	Z	0.002	-0.001	-0.015	0.022
Standard deviation of residual errors (m)	X	0.013	0.162	0.035	0.062
	Y	0.014	0.046	0.026	0.043
	Z	0.008	0.016	0.019	0.037

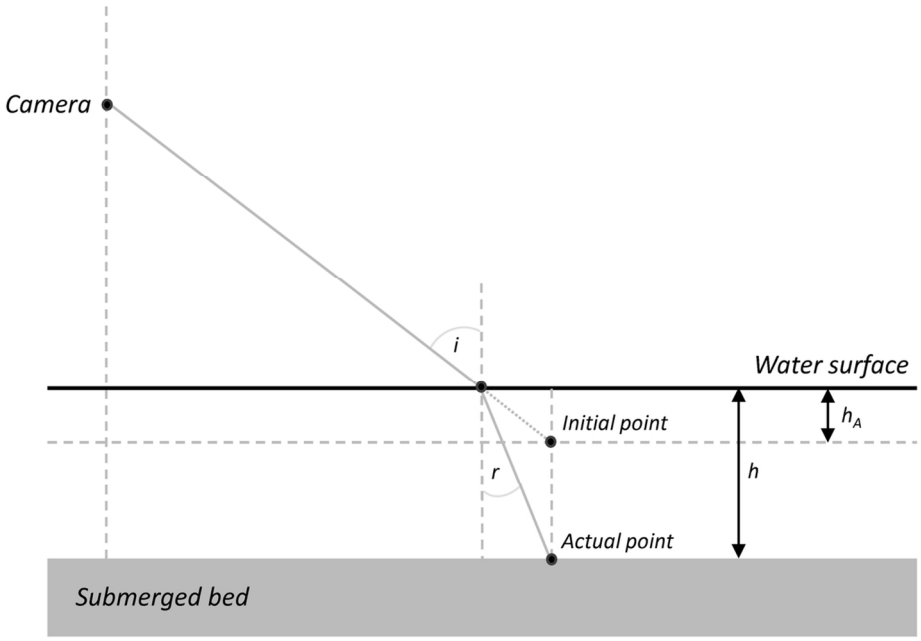

Figure 1. A schematic representation of the relationship between camera location, water surface elevation, apparent water depth (hA) and actual water depth (h) as a result of refraction at the air-water interface (after Westaway et al., 2001). Not to scale. Reproduced by permission of the American Society of Photogrammetry and Remote Sensing.
110x79mm (300 x 300 DPI)

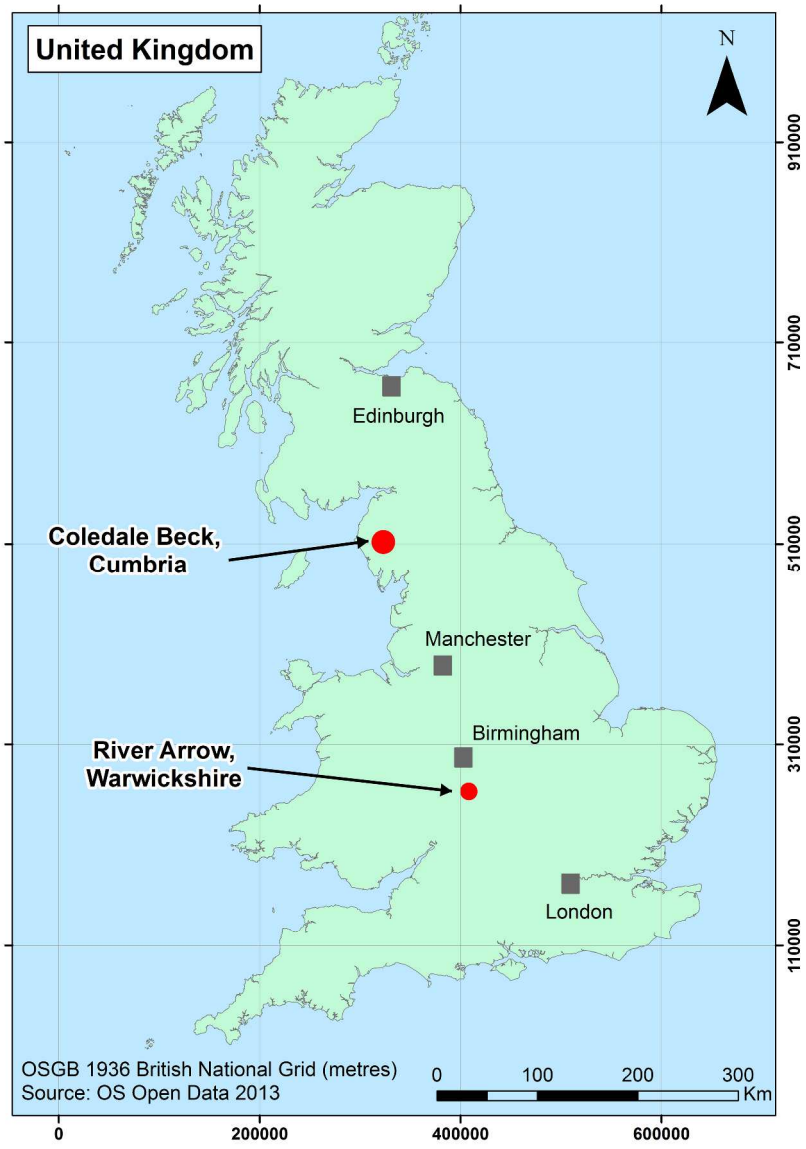

Figure 2. Location of the River Arrow and Coledale Beck sites (this figure is available in colour online).
296x419mm (300 x 300 DPI)

1. PRE-FIELD

a) Camera calibration to determine relationship between flying altitude and image resolution

2. DATA ACQUISITION

a) Distribution of GCPs
b) Image acquisition from UAS platform (multiple flights)
c) Survey position of GCPs using dGPS or total station
d) Collect independent ground validation data using dGPS or total station (including water depth where possible)

3. POST-FIELD

a) Image selection based on visual quality, view angle and altitude of images

4. SfM PROCESSING

a) Import images into PhotoScan Pro
b) Align images – identification of conjugate points to produce a sparse point cloud
c) Geometry building – densification of the point cloud
d) Texture building – raw image pixels are draped over the built geometry
e) Georeferencing – indirect georeferencing using known positions of GCPs (2c)
f) Optimise image alignment – GCP positions used to refine camera lens model and minimise geometric distortion, sparse point cloud is recomputed
g) Re-build geometry – densification of recomputed sparse point cloud
h) Re-build texture – raw images are draped over the re-built geometry
i) Export georeferenced orthophoto and DEM

5. REFRACTION CORRECTION

a) Map position of waters edge from orthophoto
b) Extract DEM values at 0.25m intervals along waters edge
c) Interpolate between DEM values using a TIN model to produce map of estimated water surface elevation
d) Subtract original DEM (4i) from estimated water surface model (5c) to give estimated water depth
e) Multiply estimated water depth (5d) by refractive index of clear water (1.34)
f) Compute difference between estimated water depth (5d) and refraction corrected water depth (5e)
g) Subtract this difference (5f) from the original DEM (4i) to give refraction corrected DEM in submerged areas

6. QUANTITATIVE DEM VALIDATION

a) Compute elevation differences between independent ground validation data (2d) and output DEMs – original (4i) and refraction corrected (5g)

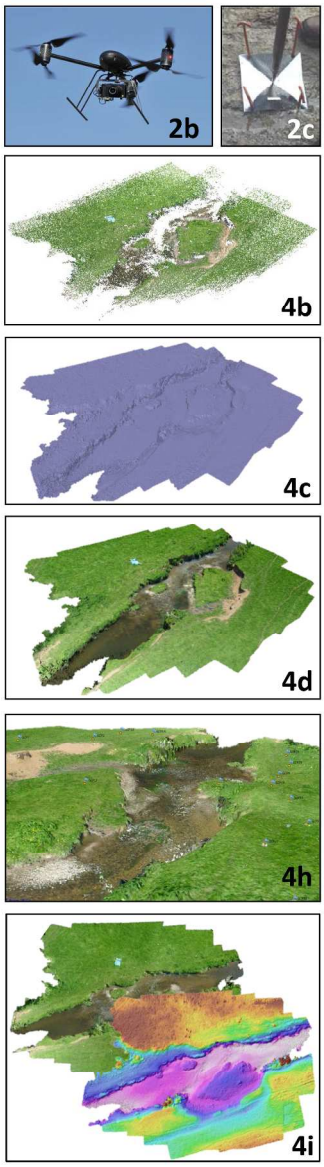

Figure 3. Workflow documenting the UAS-SfM process for production and quantitative assessment of fluvial topographic datasets (this figure is available in colour online).
254x338mm (300 x 300 DPI)

Figure 4. The Draganflyer X6 UAS (this figure is available in colour online).
75x42mm (300 x 300 DPI)

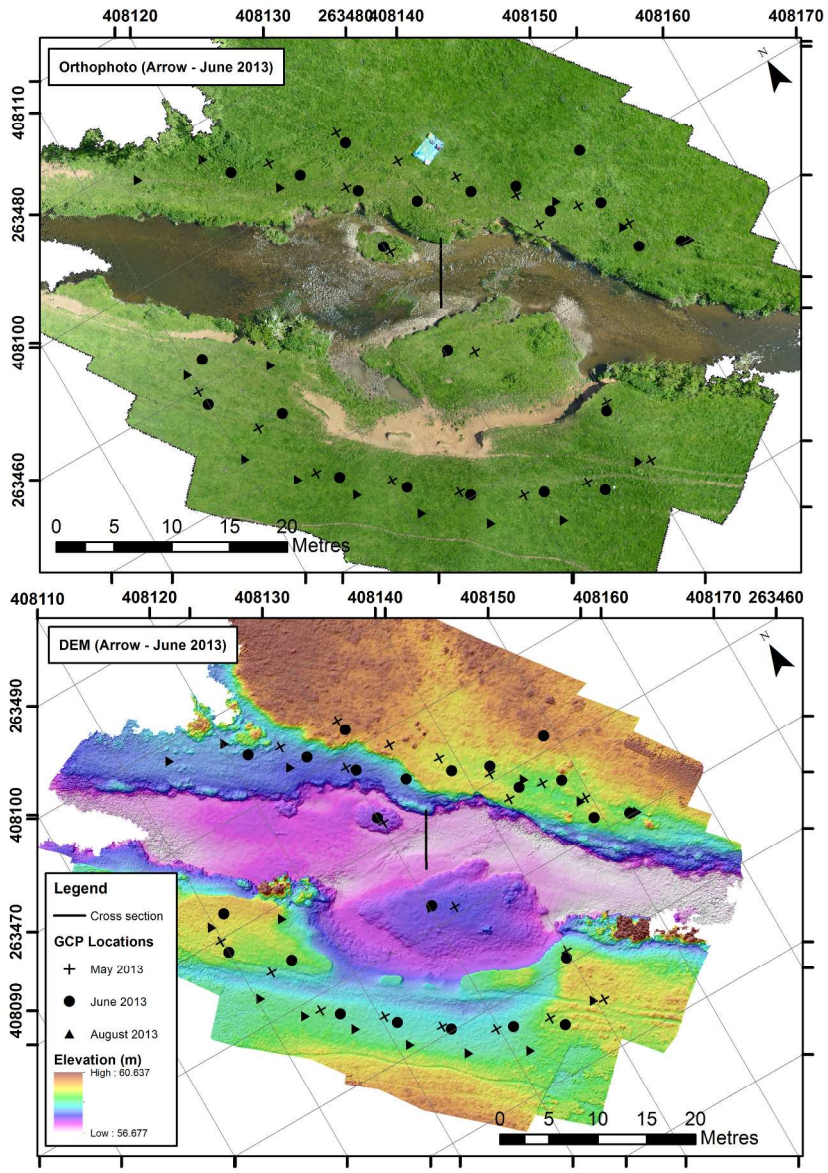

Figure 5. River Arrow orthophoto (top) and non-refraction corrected DEM (bottom) for June 2013. Black line indicates position of cross section shown in Figure 11 (this figure is available in colour online).
210x298mm (300 x 300 DPI)

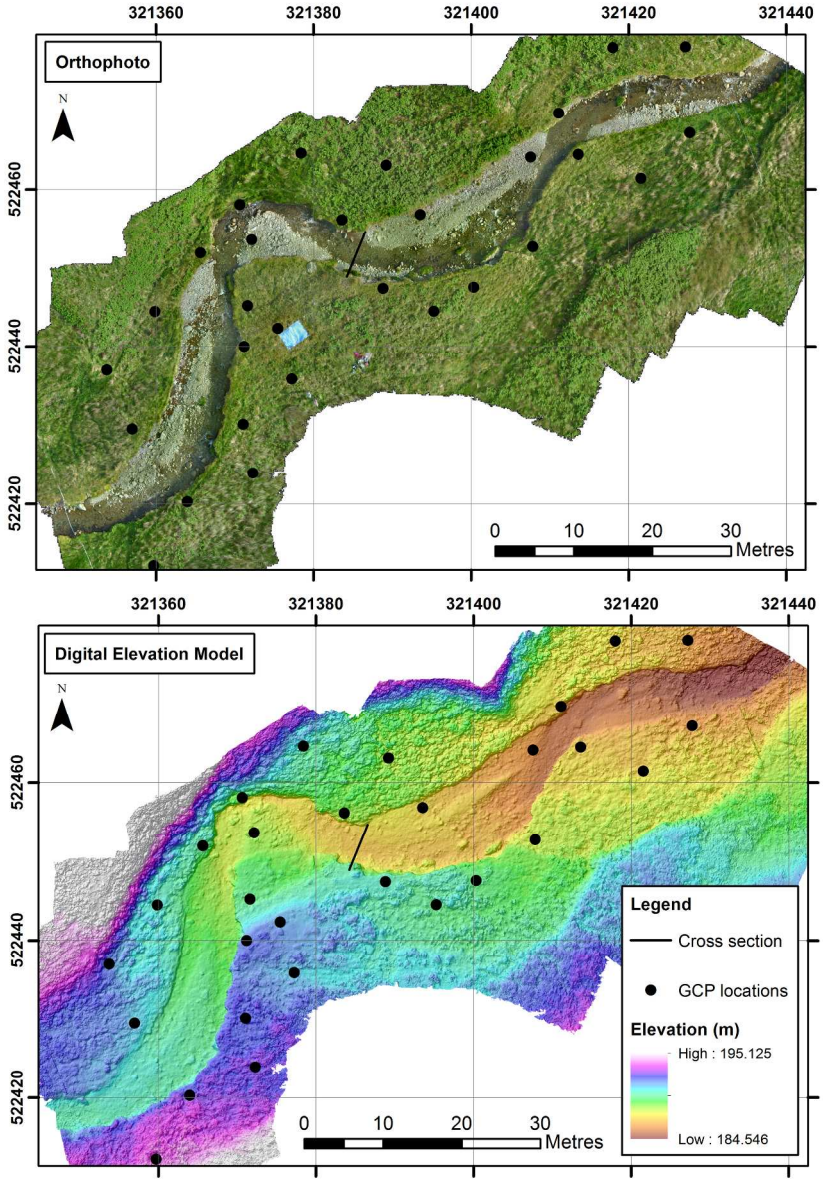

Figure 6. Coledale Beck orthophoto (top) and non-refraction corrected DEM (bottom). Black line indicates position of cross section shown in Figure 11 (this figure is available in colour online).
210x298mm (300 x 300 DPI)

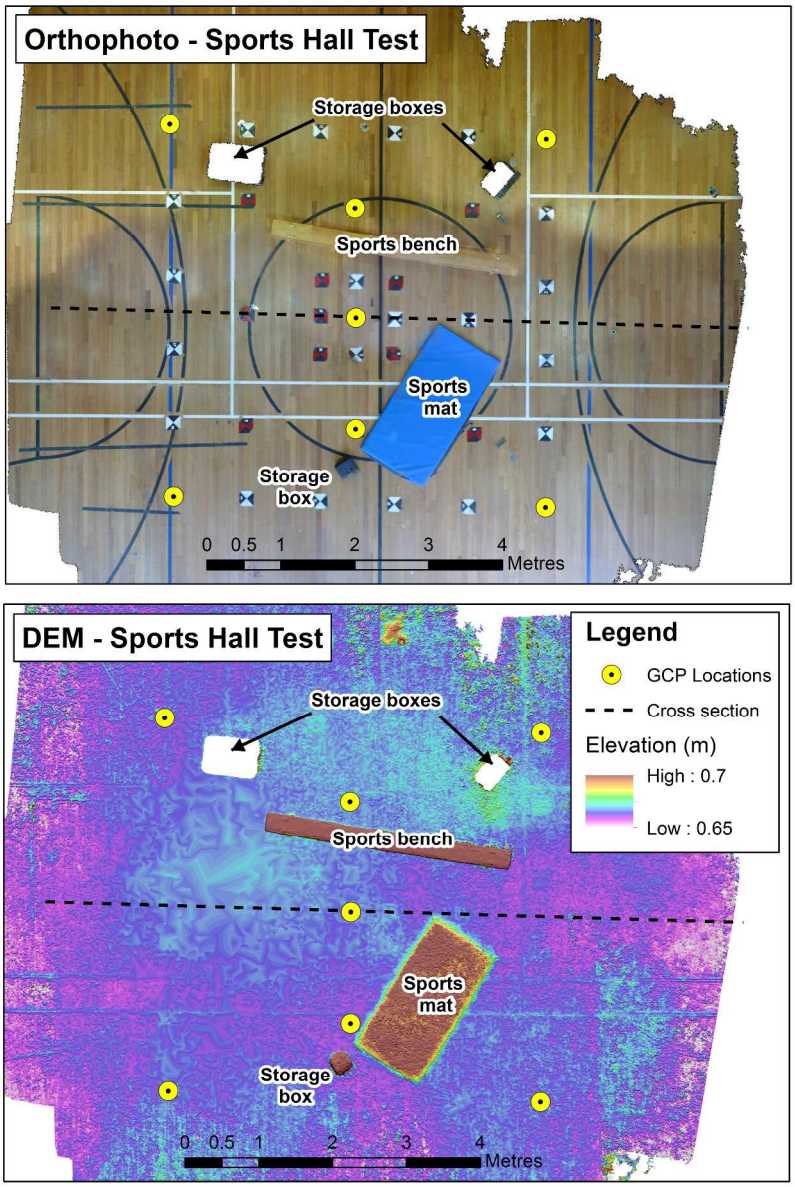

Figure 7. Sports Hall orthophoto (top) and DEM (bottom). Labels indicate the location of storage boxes and other items which were present within the scene. The dashed line indicates the location of the cross section shown in Figure 12a (this figure is available in colour online).
269x396mm (300 x 300 DPI)

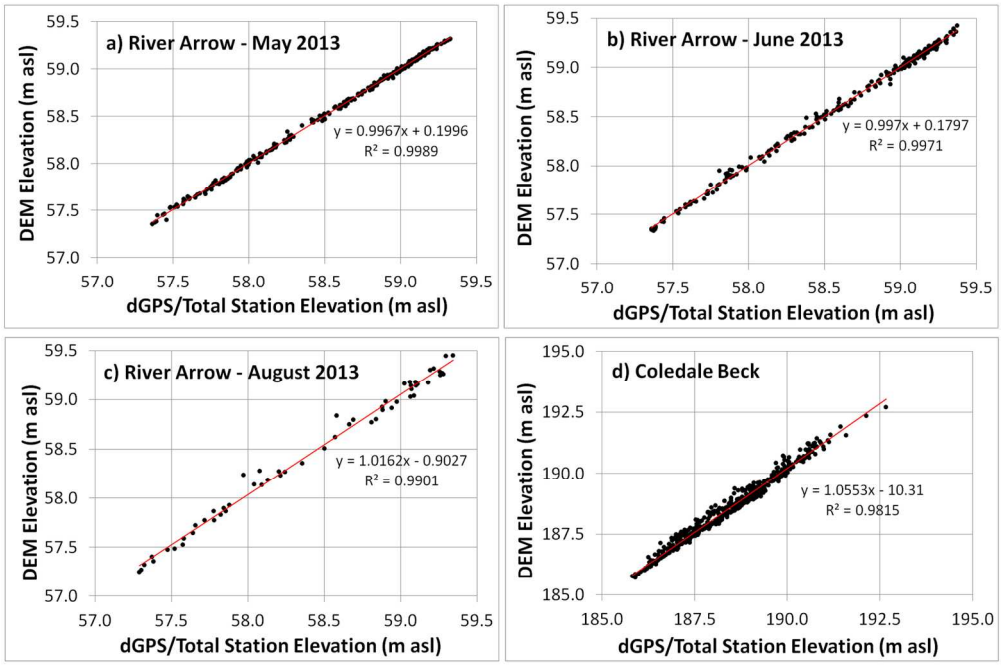

Figure 8. DEM elevations plotted against independent validation elevation values in exposed areas for a) River Arrow May 2013, b) River Arrow June 2013, c) River Arrow August 2013 and d) Coledale Beck (this figure is available in colour online).
172x117mm (300 x 300 DPI)

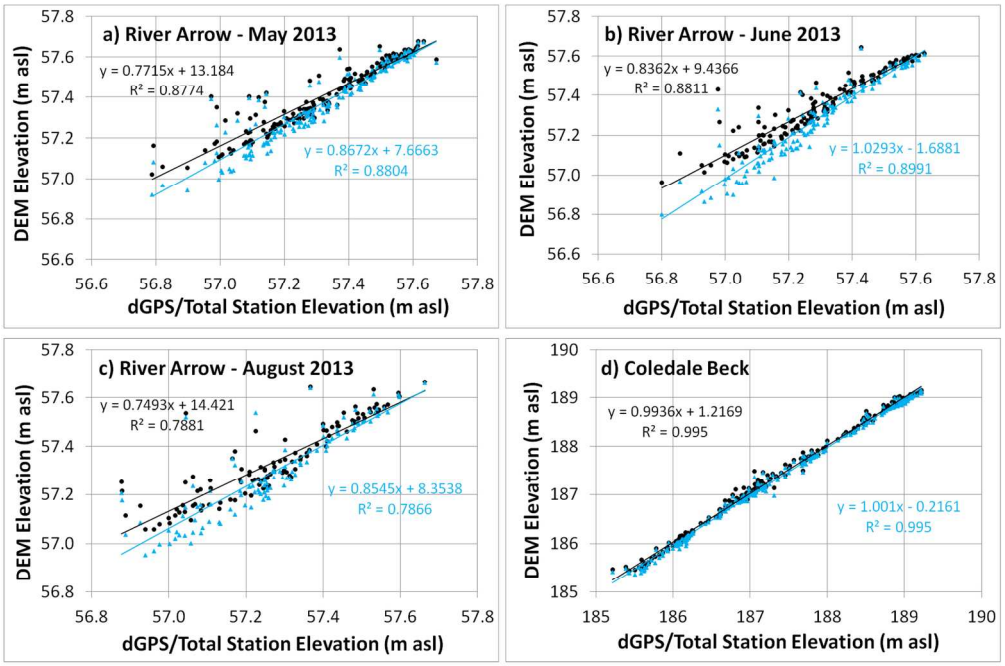

Figure 9. DEM elevations plotted against independent validation elevation values in submerged areas for a) River Arrow May 2013, b) River Arrow June 2013, c) River Arrow August 2013 and d) Coledale Beck. Black circles and lines represent non-corrected data, and blue triangles and line represent refraction corrected data (this figure is available in colour online).
174x119mm (300 x 300 DPI)

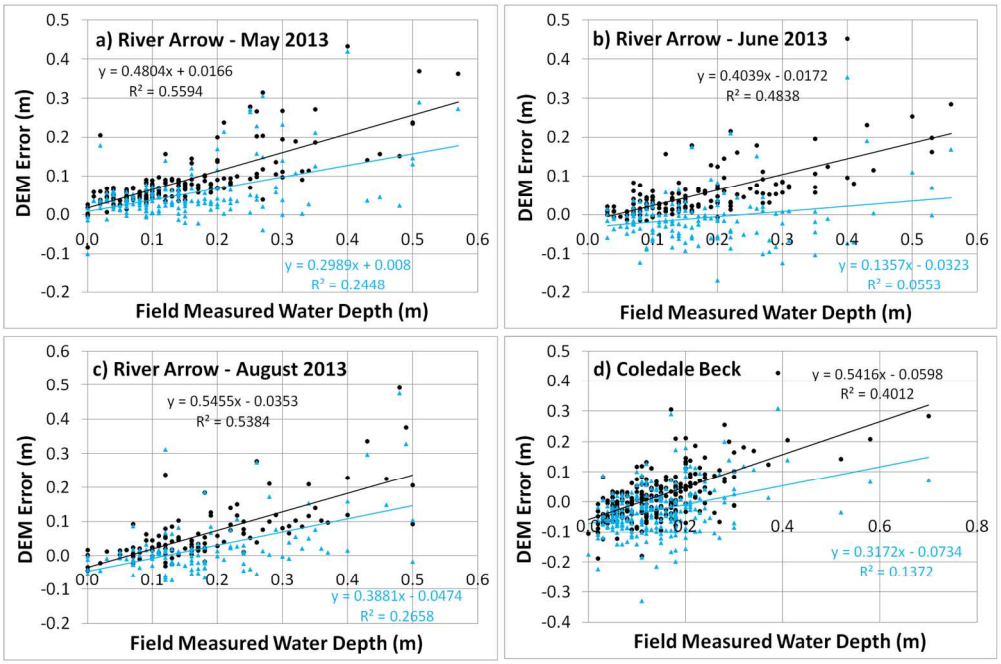

Figure 10. DEM error values plotted against field measured water depths for a) River Arrow May 2013, b) River Arrow June 2013, c) River Arrow August 2013 and d) Coledale Beck. Black circles and lines represent non-corrected data, and blue triangles and line represent refraction corrected data (this figure is available in colour online).
172x117mm (300 x 300 DPI)

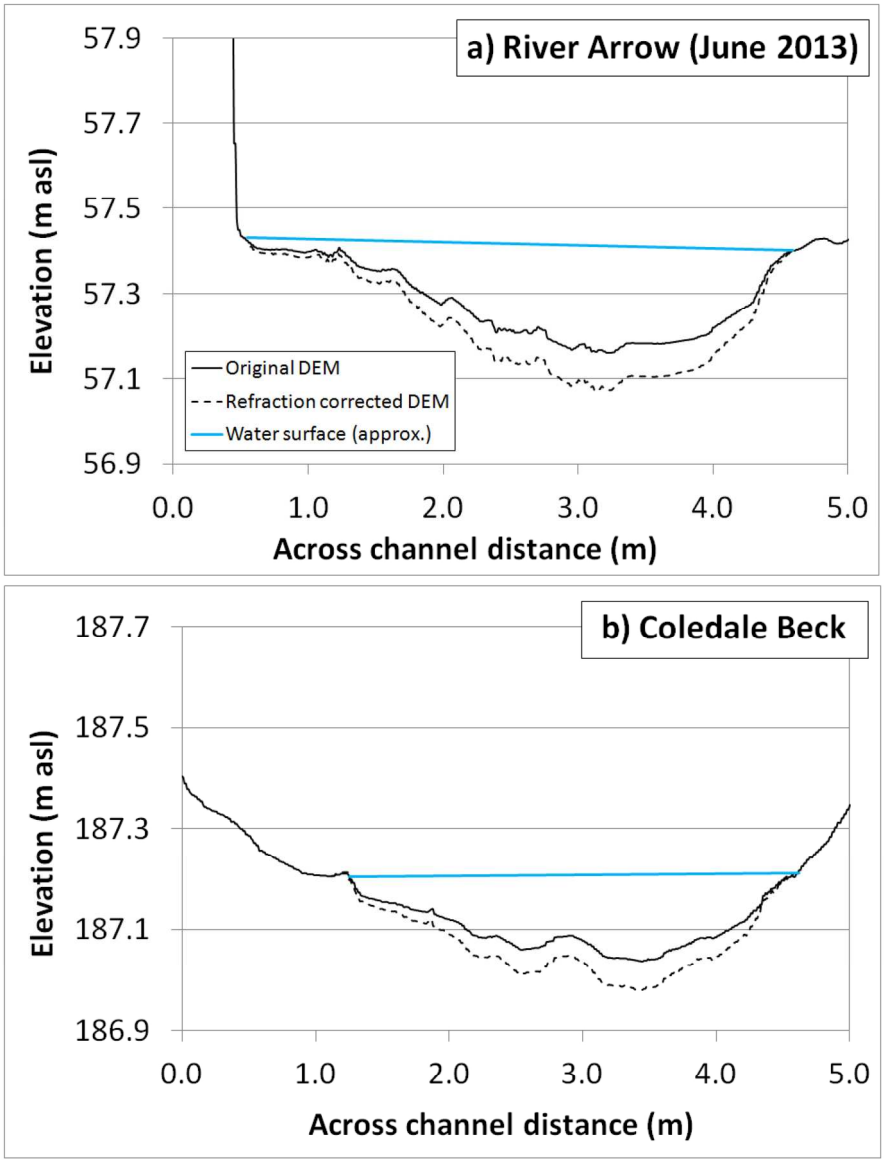

Figure 11. Example cross sections from a) River Arrow June 2013 and b) Coledale Beck, demonstrating the effects of refraction correction on channel bed elevations. The locations of these cross sections are shown on Figures 5 and 6. Water surface elevations are estimates based on the elevation at the water's edge, as described in Section 3.5 (this figure is available in colour online).
169x220mm (300 x 300 DPI)

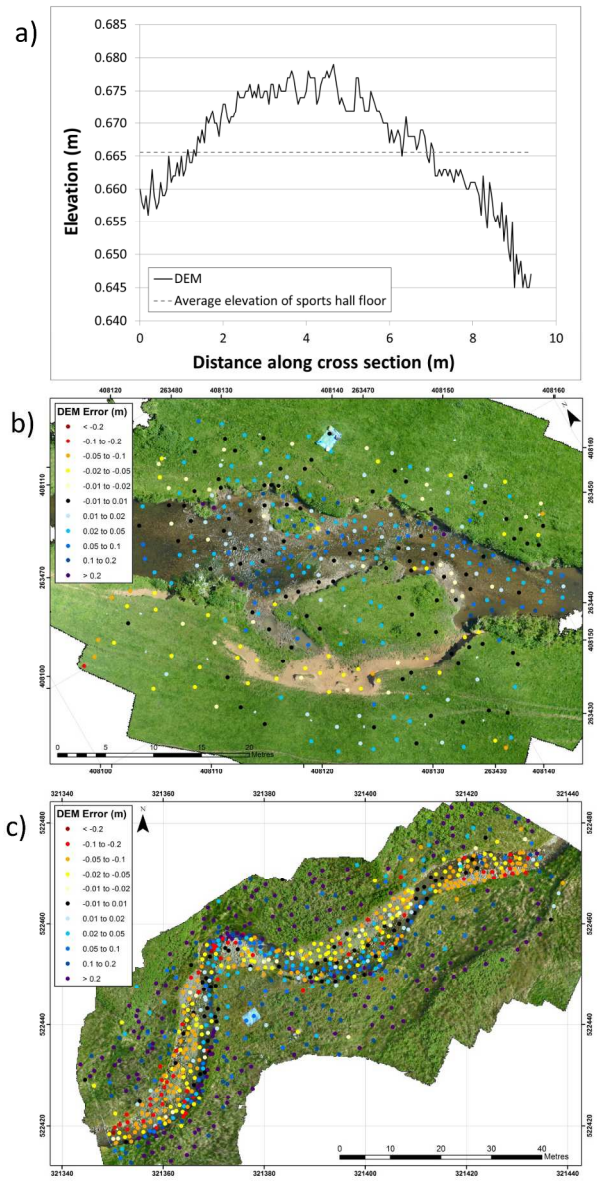

Figure 12. Spatial patterns of DEM error a) Cross section along sports hall floor, b) River Arrow June 2013 and c) Coledale Beck (this figure is available in colour online).
254x338mm (300 x 300 DPI)